ADVANCED MATERIALS

[11] J. Huang, R. B. Kaner, *Nat. Mater.* **2004**, *3*, 783.
[12] A. G. MacDiarmid, A. J. Epstein, *Synth. Met.* **1994**, *65*, 103.
[13] A. G. MacDiarmid, A. J. Epstein, *Synth. Met.* **1995**, *69*, 82.
[14] C. Visy, J. Lukkari, J. Kankare, *Macromolecules* **1994**, *27*, 3322.

All-Solution-Processed n-Type Organic Transistors Using a Spinning Metal Process**

By *Tae-Woo Lee*,* *Younghun Byun*, *Bon-Won Koo*, *In-Nam Kang*, *Yi-Yeol Lyu*, *Chang Hee Lee*, *Lyongsun Pu*, and *Sang Yun Lee**

There has been growing interest in organic thin-film transistors (OTFTs) because of their potential applications in flexible, low-cost integrated circuits, such as smart cards, RF identification tags, and display backplanes, such as liquid crystal displays, electronic paper, and organic electroluminescent displays.[1,2] In particular, since organic semiconductors based on polymers and oligomers are attractive for their easy solution processing for film formation, recent research on OTFTs has been more focused on flexible electronic devices/display applications. Therefore, the most desired ultimate goal of organic semiconductor devices is to realize flexible electronics and displays that can be processed through *all-solution processes* including deposition of the active organic layers, the gate insulators, and the electrodes. Here we demonstrate all-solution-processed n-type organic transistors for the first time by depositing the source and drain metal by a spinning metal process.

Despite the great interest and progress in organic and polymeric TFTs, most of the high field-effect-mobility OTFTs have been based on p-type channel materials. However, even if n-channel semiconducting materials are important for making ambipolar transistors[3,4] and complementary circuits,[5] they are relatively rare compared with the p-type materials. The reported field-effect mobilities of n-type OTFTs to date also show lower values than those of p-type devices. In addition, it has usually been observed that the solution-processed OTFTs show poorer performance than the vacuum-processed devices: for example, although the vacuum-evaporated pentacene transistor has shown high field-effect hole mobilities exceeding 1 $cm^2 V^{-1} s^{-1}$,[6] the solution-processed p-type transistor using the pentacene precursor showed low field-effect mobilities below 0.1 $cm^2 V^{-1} s^{-1}$.[7] Reports about the solution-processed n-type transistors are also relatively rare[5,8–10] and they usually show low charge-carrier mobilities (~10^{-2} $cm^2 V^{-1} s^{-1}$ or less)[5,8,10,11] except that most recently the observation of a field-effect electron mobility as high as 0.1 $cm^2 V^{-1} s^{-1}$ for a solution spin-coated conjugated ladder polymer was reported.[9] Here we report on solution-processed n-type OTFTs with high field-effect mobilities, based on the soluble derivatives of fullerene (C_{60}) as n-type channel materials. We obtained high field-effect electron mobilities of 0.02–0.1 $cm^2 V^{-1} s^{-1}$ depending on the work-function of the source and drain metals, demonstrating that the electron injection current is contact-limited because of the Schottky barrier at the contact.

Furthermore, we fabricated n-type OTFTs by an all-solution-deposition process including source and drain metals as well as gate insulators and organic semiconductors. These types of OTFTs are well suited for a wide range of existing and future flexible circuits and display applications that require a simplified production process and low-weight and low-cost products. In order to achieve the solution-processed organic semiconductor film in the OTFTs, we used a thermally curable organic gate insulator. Before spin-coating the organic semiconductor, we deposited highly photosensitive organosilver precursor solutions on top of the organic gate insulator and patterned the films to form reduced silver metal by irradiating with broadband UV light through a photomask.

The organic semiconductor materials used in this work, which are soluble derivatives of C_{60} are shown in Figure 1a: Fulleroid (1-(3-methoxycarbonyl) propyl-1-phenyl[5,6]C61) (F[5,6]) and methanofullerene 1-(3-methoxycarbonyl)propyl-1-phenyl[6,6]C61 (M[6,6]). The OTFT structures used are shown in Figure 1b. We fabricated both top-contact (left of Fig. 1b) and bottom-contact (right of Fig. 1b) geometry devices.

The soluble C_{60} derivatives were spin-cast from a chlorobenzene (CB) solution. The cast films were smooth and clear. The root-mean-square (RMS) roughness of the films range from 1.9 to 2.24 nm, depending on the spin speed, and are good enough for device fabrication. The morphology of the M[6,6] film is shown in Figure 2. Interestingly, the surface morphologies are strongly dependent on the spin speed, as shown in Figure 2. When we spun the ~1 wt. % CB solution at 1000 rpm, we obtained ~100 nm thick films with a 2.24 RMS roughness. The surface morphology shows a kind of aggregation of the molecules: the morphology of films spin-cast at 1000 rpm

[*] Dr. T.-W. Lee, Dr. S. Y. Lee, Dr. Y. Byun, Dr. B.-W. Koo, Y.-Y. Lyu, Dr. L. Pu
Samsung Advanced Institute of Technology
Mt. 14-1, Nongseo-Ri, Giheung-Eup
Yongin-Si, Gyeonggi-Do, 449-712 (Korea)
E-mail: taew.lee@samsung.com; sangyoon.lee@samsung.com
Prof. I.-N. Kang
Department of Chemistry
The Catholic University of Korea
43-1 Yeokgok 2-dong, Wonmi-gu
Bucheon-Si, Gyeonggi-do, 420-743 (Korea)
Prof. C. H. Lee
School of Electrical Engineering and Computer Science
Seoul National University
Seoul 151-744 (Korea)
Dr. L. Pu
Dept. of Advanced Materials
Sungkyunkwan University
300 Chunchun-Dong, Jangan-Gu
Suwon, Kyunggi-Do, 440-746 (Korea)

[**] The authors acknowledge Dr. R. R. Das for the careful reading of the manuscript.

  DOI: 10.1002/adma.200401672

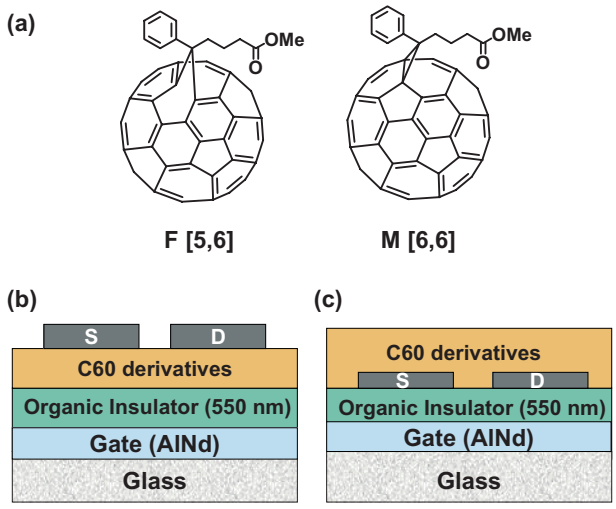

Figure 1. a) Chemical structures of the soluble fullerene derivatives used in the OTFTs. Fulleroid (1-(3-methoxycarbonyl)propyl-1-phenyl[5,6]C61) (F[5,6]) (left) and methanofullerene 1-(3-methoxycarbonyl)propyl-1-phenyl[6,6]C61 (M[6,6]) (right). b) The structure of a top-contact OTFT with a deposited AlNd gate on glass, a curable organic insulator (550 nm), soluble fullerene derivatives, and source–drain metal electrodes in sequence from bottom to top. c) The structure of a bottom-contact OTFT with a deposited AlNd gate on glass, a curable organic insulator (550 nm), source–drain metal electrodes, and soluble fullerene derivatives in sequence from bottom to top.

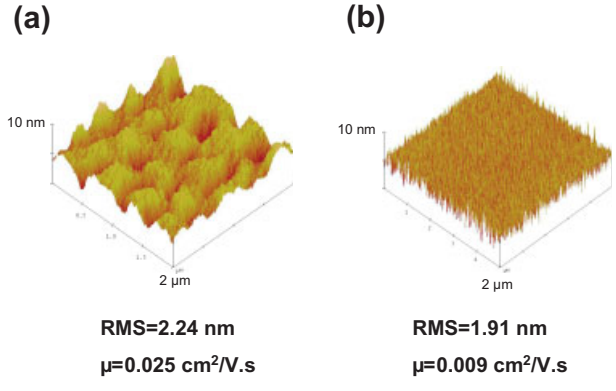

Figure 2. a) Atomic force microscopy image of a thin film spin cast at 1000 rpm from a ~1 wt.-% M[6,6] solution in CB. The film surface shows that the molecules are aggregated. The RMS surface roughness is 2.24 nm. The field-effect electron mobility of the top-contact transistor device with the Au source–drain metal electrode is 0.025 $cm^2 V^{-1} s^{-1}$. b) Atomic force microscopy image of a thin film spin cast at 2000 rpm from a ~1 wt.-% M[6,6] solution in CB. The film shows a smoother surface (RMS surface roughness: 1.91 nm) than that spin cast at 1000 rpm. The field-effect electron mobility of the top-contact transistor device with the Au source–drain metal electrode is 0.009 $cm^2 V^{-1} s^{-1}$.

looks like a periodic array of bulky ball patterns, indicating that the molecules aggregate to form the thermodynamically more stable form (bulky ball-like shape) wherein the molecules could be orderly packed. However, when the solution was spun at 2000 rpm, no such aggregation was observed (RMS roughness: 1.91 nm). Although the slower spin speed could provide more time for the molecules to aggregate during the solvent-drying time, the higher spin speed does not provide enough time for aggregation or ordering. Generally, the field-effect mobility decreases as the thickness of the channel layer increases because of the higher serial resistance.[12] However, it is worth noting that the aggregated film (a thicker film (~110 nm) spun at 1000 rpm) gave a higher field-effect electron mobility (0.025 $cm^2 V^{-1} s^{-1}$ at a gate voltage, $V_g = 18.5$ V) than the non-aggregated film (a thinner film (~70 nm) spun at 2000 rpm) (0.009 $cm^2 V^{-1} s^{-1}$ at $V_g = 29.5$ V) for the top-contact Au-based device (see Fig. 1b). This indicates that the close packing and aggregation of the molecules increase the charge-carrier mobility in the transistor. In other reports in the literature, the aggregation is usually regulated by heating the films or varying the solvents.[12,13] However, our results suggest that the aggregation of small molecules can be regulated by the spinning conditions in order to increase the charge carrier mobility of the films. Films of F[5,6] showed a similar surface morphology and electron mobility to those of M[6,6]. Therefore, it can be concluded that the aggregated films of this kind can give higher charge-transport mobility.

The OTFTs of both F[5,6] and M[6,6] showed quite similar current–voltage characteristics. Figure 3a shows the transfer characteristics of TFTs based on both materials with a polymer gate dielectric layer and Au top contacts, in which F[5,6] and M[6,6] were spin cast at 1000 rpm. Both device field-effect mobilities were essentially the same (0.025 $cm^2 V^{-1} s^{-1}$) and the threshold voltages were also the same (13.6 V). The mobility was obtained from the slope in the plot of the square root of the source–drain current versus gate voltage. Since we used an unpatterned gate electrode, the region of the source and drain electrodes overlapped with that of the gate electrode (see Fig. 1). Hence, the gate leakage increases as the gate voltages increases, which can explain why the slope in the square root of the source–drain current versus voltage plot tends to strongly decrease above 30 V, as seen in Figure 3a. The on/off ratio of the devices was ~4000. The field-effect mobility achieved here is higher than the mobility values reported in previous literature on the electron mobility in diodes and transistors utilizing soluble C_{60} derivatives.[3,9,11] This is possibly a result of the controlled aggregate morphology of the film, achieved by regulating the spin speed. The energy of the lowest unoccupied molecular orbital (LUMO) of these soluble C_{60} derivatives is 3.7 eV and that of the highest occupied molecular orbital (HOMO) is 6.1 eV. Since we used the high-workfunction Au (~5.1 eV) metal for the source–drain contact, the electron injection current can be limited by the contacts. Therefore, we tried to observe the dependency of the field-effect electron mobility on the workfunction of other source–drain metals. It was observed that the field-effect mobility in the transistor linearly increases as the metal workfunction decreases (see Fig. 3b) and reaches a maximum value of ~0.1 $cm^2 V^{-1} s^{-1}$ with the Ca electrodes. To the best of our knowledge, this is the highest field-effect electron mobility among solution-processed organic transistors based on non-polymeric n-type small molecules and is comparable to the

ADVANCED MATERIALS

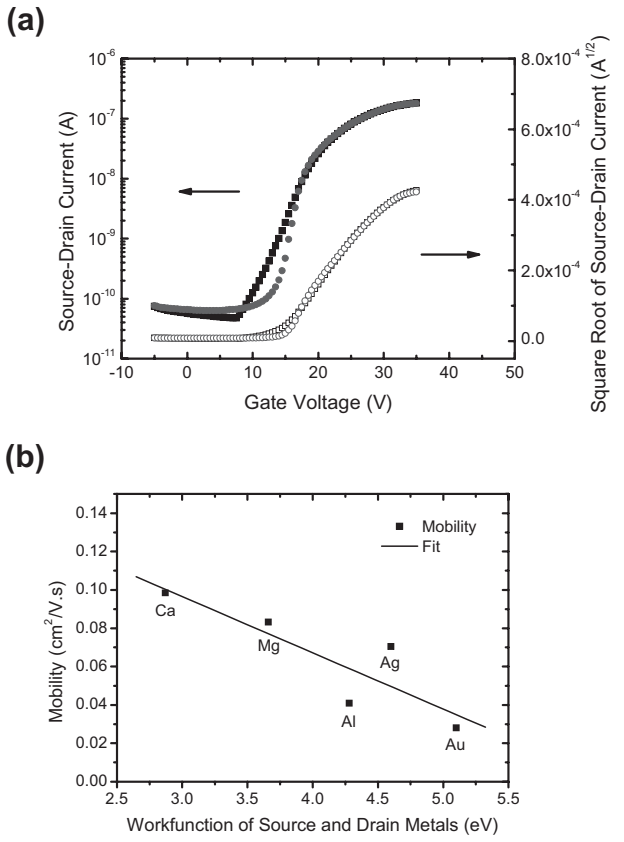

Figure 3. a) Transfer characteristics of the thin-film n-type transistors with Au electrodes based on F[5,6] (squares) and M[6,6] (circles). The devices are driven at a source–drain voltage (V_d) of 20 V. F[5,6] and M[6,6] were spin-cast at 1000 rpm spin speed. Both device mobilities were essentially the same (0.025 $cm^2 V^{-1} s^{-1}$). The transfer characteristics show that the threshold voltages of both the devices were also the same (13.6 V). b) Field-effect mobility versus the workfunction of source–drain metals used for top-contact OTFTs. The solid line indicates the line fitted using linear regression.

most recently reported high-electron-mobility n-type polymer transistors.[9] The increase of the field-effect mobilities with decreasing workfunction demonstrates that the electron current is contact-limited because of the Schottky barrier at the contact. Therefore, the field-effect mobility of the n-type transistor using a low-workfunction metal such as Ca could be close to the intrinsic mobility of a thin film of the n-type material.

We fabricated the n-type transistors by solution deposition of all layers including deposition of the source–drain metals, organic gate insulator, and organic semiconductor. The organic gate insulator and the semiconductor can be spin cast from cyclohexanone and CB solutions, respectively. The solution-deposition method of the source–drain metals was newly developed by our group. This is a silver-patterning method in which the spin-cast highly photosensitive organosilver precursors are reduced to Ag metal by UV irradiation through a photomask. The procedure is illustrated in Figure 4a. The photosensitive organosilver precursors were prepared by the reaction of silver salts and excess amines. The photosensitive silver precursor was spin cast on top of the organic insulator/AlNd substrate to form an amorphous film followed by broadband UV exposure of the film through the photomask. This produced a partially reduced silver compound within 5 min, which was insoluble in MeCN. After developing with the solvent, the irradiated areas were reduced by hydrated hydrazine to obtain pure metallic patterns and then thermally annealed at a moderate temperature (80–100 °C for 5 min) to increase the adhesion of the interface and cohesion of the silver particles. We finally obtained 70–80 nm thick Ag metal source–drain patterns, as shown in Figure 4. Figure 4b shows one of the scanning electron microscopy images of the thus obtained metal patterns. Although the usual metal shadow evaporation does not give the well-defined sharp features on the edge of the patterns, we can clearly observe the well-defined channel between the source and the drain. Since this method is basically based on a photolithography process, we can also fabricate short-channel devices with lengths below 5 μm, which are usually difficult to fabricate with conventional shadow-mask evaporation. The atomic force microscopy pictures of the source and the drain metal indicates an RMS roughness value of 4.76 nm (Fig. 4c), which is slightly higher than the RMS surface roughness (1.82 nm) of sputter-deposited Ag films on glass.

We characterized the fabricated devices and compared them to devices fabricated by the vacuum thermal deposition process. The all-solution-processed M[6,6] device in the bottom-contact structures of the 50 μm length (L) and 2 mm width (W) channel with Ag metal showed a 0.003 $cm^2 V^{-1} s^{-1}$ mobility at $V_g = 25$ V (see Fig. 5). This is much higher than the mobility (0.0007 $cm^2 V^{-1} s^{-1}$ at $V_g = 29$ V) of the conventional bottom-contact device with the vacuum-deposited Ag metal. Although we do not clearly understand the reason for the improved performance of the transistor formed using solution deposition of the source–drain metal electrodes, it could possibly result from less damage to the organic insulator interface than that caused by metal vacuum evaporation, as suggested in previous literature.[15,16] In comparison with the top-contact devices, the bottom-contact devices showed a much lower field-effect mobility. This implies that the contact problem is much more dominant in the bottom-contact devices. The off current of the solution-processed device is higher than the vacuum metal-deposited device, which may result from gate or channel leakage by the impurities generated during the photopatterning process. Therefore, we are trying to remove these impurities by modifying the development process or by adding an additional washing process. Although we applied our solution metal process to an n-type organic transistor, this method can be also employed to fabricate all-solution-processed p-type organic transistors.

In summary, we fabricated a high-mobility solution-processed n-type transistor using soluble fullerene derivatives. When we prepared the films of the fullerene derivatives at a low spinning speed, the film showed an aggregated morphology, which imparted a high field-effect electron mobility to the organic transistor devices. The field-effect electron mobil-

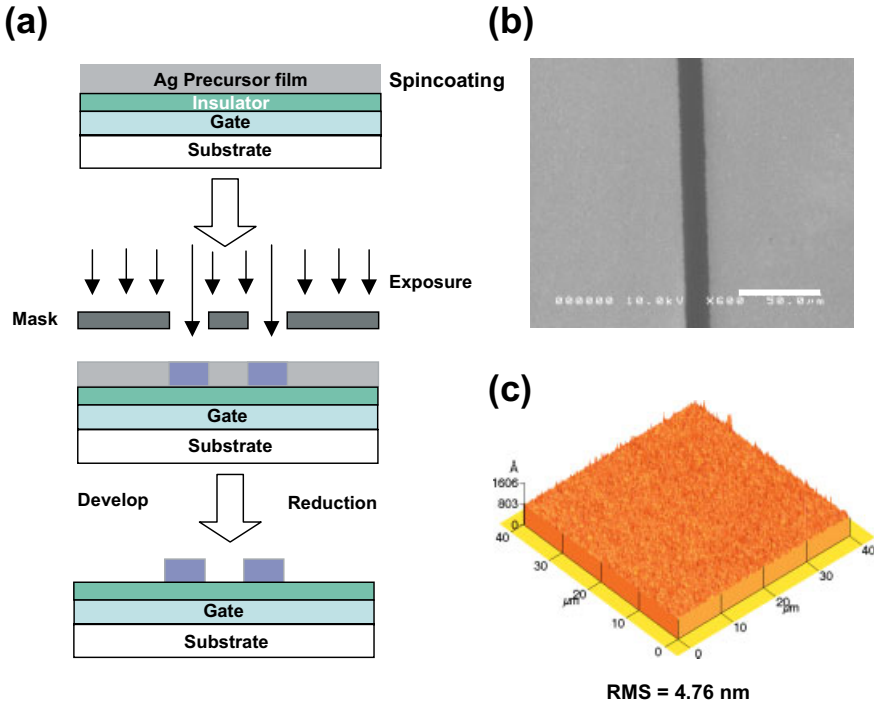

Figure 4. a) The procedure for the deposition of patterned source–drain metals with solution organosilver precursor. The photosensitive organosilver precursor is spin-coated onto the top of the insoluble thermally cured organic insulator (a polyvinylphenol derivative)/AlNd gate/glass substrate. The broadband UV irradiation of the film through a photomask produces a partially reduced and insoluble silver compound. After developing with MeCN, the irradiated areas can be reduced by hydrated hydrazine to obtain pure source–drain metallic patterns (70–80 nm). b) Scanning electron microscopy image of the resulting source–drain pattern with 15 μm channel length. The scale bar is 50 μm. c) Atomic force microscopy image of the reduced metallic patterns, showing an RMS roughness of 4.76 nm.

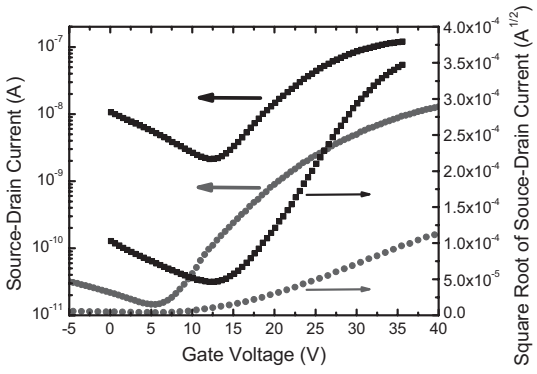

Figure 5. Transfer characteristics of all-solution-processed TFTs of M[6,6] with Ag electrodes in the bottom-contact geometry fabricated by the solution silver precursor route (■) (channel length = 100 μm, channel width = 1 mm) as well as the regular vacuum deposition (●) (channel length = 50 μm, channel width = 2 mm). The devices are driven at a source–drain voltage of 20 V. M[6,6] was spin cast at 1000 rpm. The field-effect transistor fabricated via a solution silver precursor route shows a higher electron mobility (0.003 $cm^2 V^{-1} s^{-1}$) than that obtained via conventional shadow vacuum deposition (0.0007 $cm^2 V^{-1} s^{-1}$).

ity of the solution-processed fullerene derivatives with various top metal contacts ranged from 0.02 to 0.1 $cm^2 V^{-1} s^{-1}$, depending on the metal workfunction. The value of 0.1 $cm^2 V^{-1} s^{-1}$ is, to the best of our knowledge, the highest electron mobility among solution-processed organic transistors based on non-polymeric n-type small molecules. Finally, we successfully fabricated all-solution-processed n-type organic transistors by depositing the source–drain metal electrodes using a solution metal precursor route. The devices fabricated in this manner showed a higher electron mobility than the devices fabricated by vacuum shadow deposition. This all-solution process for OTFTs is useful to fabricate low-cost, flexible integrated circuits and display backplanes.

Experimental

Synthesis of Fullerene Derivatives: The soluble fullerene derivatives, Fulleroid (1-(3-methoxycarbonyl)propyl-1-phenyl[5,6]C61) (F[5,6]) and methanofullerene 1-(3-methoxycarbonyl)propyl-1-phenyl[6,6]C61 (M[6,6]) were synthesized according to the previous literature [17].

Preparation of Organosilver Precursor (n-$PrNH_2$)$Ag(NO_2)\cdot 0.5CH_3CN$: To a solution of $AgNO_2$ (1.53 g, 10 mmol) in 20 mL of CH_3CN was added excess *n*-propylamine (3.60 g, 60 mmol) dropwise in the absence of light. Stirring the reaction mixture for 4 h at room temperature resulted in a small amount of brown precipitate and a pale yellow solution. The reaction mixture was filtered by a 0.2 μm polyTFE membrane filter. The filtrate was reduced in volume to ~5 mL, followed by the addition of 50 mL of Et_2O (Et: ethyl). This solution was filtered again, and all volatile materials were removed under vacuum at room temperature to afford a light yellow oil (1.9 g). ^1H NMR (CD_3CN, ppm): 2.69 (t, 2H, N-CH_2), 1.50 (m, 2H, CH_2CH_3),

ADVANCED MATERIALS

0.90 (t, 3H, CH_2CH_3). Anal. Calcd. for $C_3H_9N_2O_2Ag{\cdot}0.5CH_3CN$: C 20.57, H 4.53, N 15.00 %. Found: C 19.81, H 4.51, N 14.82 %.

Device Fabrication and Measurement: The thermally crosslinkable organic gate insulator, a thermally crosslinkable polyvinylphenol derivative (Samsung proprietary), was spin cast from cyclohexanone solution on top of the AlNd gate substrate and then cured on a hot plate at 150 °C for 1 h. The thickness of the organic insulator was ~550 nm. After thermal curing, the organic insulator was insoluble in organic solvents. To fabricate a top-contact transistor, the soluble fullerene derivatives were spin cast from the chlorobenzene solution to form a 70–110 nm thick layer (1000–2000 rpm with ~1 wt.-% solution) and then dried on a hot plate at 70–80 °C for 3 h under vacuum. The source–drain metals (Ca, Mg, Al, Ag, and Au) were then deposited by vacuum shadow evaporation to complete the device. 250 nm thick Al and Ag protective layers were deposited to prevent oxidation on top of the 10 nm Ca and Mg, respectively. Practically all of the fabrication process was performed under an inert (N_2) atmosphere and vacuum to avoid exposure of the fullerene derivatives to air. The device test was performed immediately after the device fabrication in air and was finished in no more than 30 min. To fabricate a bottom-contact device, the source–drain metal electrodes were deposited on top of the organic insulator before the deposition of the organic semiconductor. We did not perform any surface treatment on the source–drain metal electrodes in bottom-contact geometry. For the bottom- and top-contact geometry, the channel length (L) was 100 μm and the channel width (W) was 1 mm. Source–drain currents were measured using a Keithley Semiconductor Analyzer (4200-SCS). The source–drain current (I_D) is governed by the equation:

$$I_D = \frac{WC_i\mu}{2L}(V_G - V_T)^2 \quad (1)$$

where C_i is the capacitance per unit area of the gate insulator layer, V_G is the gate voltage, V_T is the threshold voltage, and μ is the field-effect mobility. The mobility (μ) was calculated from the slope of the plot of $(|I_D|)^{1/2}$ versus V_G in the saturation regime.

Received: October 11, 2004
Final version: April 18, 2005
Published online: August 8, 2005

[1] G. Horowitz, *Adv. Mater.* **1998**, *10*, 365.
[2] H. E. Katz, *J. Mater. Chem.* **1997**, *7*, 369.
[3] E. J. Meijer, D. M. De Leeuw, S. Setayesh, E. Van Veenendaal, B.-H. Huisman, P. W. M. Blom, J. C. Hummelen, U. Scherf, T. M. Klapwijk, *Nat. Mater.* **2003**, *2*, 678.
[4] T. D. Anthopoulos, C. Tanase, S. Setayesh, E. J. Meijer, J. C. Jummelen, P. W. M. Blom, D. M. de Leeuw, *Adv. Mater.* **2004**, *16*, 2174.
[5] H. E. Katz, A. J. Lovinger, J. Johnson, C. Kloc, T. Siegrist, W. Li, Y.-Y. Lin, A. Dodabalapur, *Nature* **2000**, *404*, 478.
[6] T. W. Kelley, L. D. Boardman, T. D. Dunbar, D. V. Muyres, M. J. Pellerite, T. P. Smith, *J. Phys. Chem. B* **2003**, *107*, 5877.
[7] A. Afzali, C. D. Dimitrakopoulos, T. O. Graham, *Adv. Mater.* **2003**, *15*, 2066.
[8] C. Waldauf, P. Schilinsky, M. Perisutti, J. Hauch, C. J. Brabec, *Adv. Mater.* **2003**, *15*, 2084.
[9] A. Babel, S. A. Jenekhe, *J. Am. Chem. Soc.* **2003**, *125*, 13 656.
[10] A. Babel, S. A. Jenekhe, *Adv. Mater.* **2002**, *14*, 371.
[11] V. D. Mihailetchi, J. K. J. van Duren, P. W. M. Blom, J. C. Hummelen, R. A. J. Jassen, J. M. Kroon, M. T. Rispens, W. J. H. Verhees, M. M. Wienk, *Adv. Funct. Mater.* **2003**, *13*, 43.
[12] J. Lee, K. Kim, J. H. Kim, S. Im, D.-Y. Jung, *Appl. Phys. Lett.* **2003**, *82*, 4169.
[13] A. R. Murphy, J. M. J. Fréchet, P. Chang, J. Lee, V. Subramanian, *J. Am. Chem. Soc.* **2004**, *126*, 1596.
[14] J.-F. Chang, B. Sun, D. W. Breiby, M. M. Nielsen, T. I. Sölling, M. Giles, I. McCulloch, H. Sirringhaus, *Chem. Mater.* **2004**, *16*, 4772.
[15] J. Zaumseil, T. Someya, Z. Bao, Y.-L. Loo, R. Cirelli, J. A. Rogers, *Appl. Phys. Lett.* **2003**, *82*, 463.
[16] T.-W. Lee, J. Zaumseil, Z. Bao, J. W. P. Hsu, J. A. Rogers, *Proc. Natl. Acad. Sci. USA* **2004**, *101*, 429.
[17] J. C. Hummelen, B. W. Knight, F. LePeq, F. Wudl, *J. Org. Chem.* **1995**, *60*, 532.

Enhancement of Surface-Relief Gratings Recorded on Amphiphilic Liquid-Crystalline Diblock Copolymer by Nanoscale Phase Separation

By *Haifeng Yu*, *Kunihiko Okano*, *Atsushi Shishido*, *Tomiki Ikeda*,* *Kaori Kamata*, *Motonori Komura*, and *Tomokazu Iyoda*

Holographic gratings can be recorded on both amorphous and liquid-crystalline (LC) polymers through photoisomerization or photochemical phase transition of chromophores,[1–7] and have potential applications in information technology.[3–11] Generally, the diffraction efficiency (DE) is one of the most important parameters for holographic gratings, whose control and stability have become the focus of scientific research. Alteration of the chemical structure of materials has often been adopted, although it requires a large amount of synthetic work. Recently, gain effects,[4] mechanical stretch,[6a] electrical switch,[12] self-assembly,[6b] mixing with liquid crystals,[7a] and crosslinking[7b] have been explored to improve the DE. However, the technique of phase separation has not yet been adopted. Although this method may be simple and effective, phase separation is usually micrometer- or submicrometer-scaled and cannot be applied directly due to serious scattering of visible light, which decreases the DE. If the phase domain size is reduced to the nanoscale, e.g., smaller than 100 nm, scattering can be eliminated.

Recently, we have reported a series of novel amphiphilic LC diblock copolymers (ALDCs) consisting of flexible poly(ethylene oxide) (PEO) as a hydrophilic segment and poly(methacrylate) containing an azobenzene (AZO) moiety

[*] Prof. T. Ikeda, Dr. H. Yu, K. Okano, Dr. A. Shishido, Dr. K. Kamata, Dr. M. Komura, Prof. T. Iyoda
Chemical Resources Laboratory, Tokyo Institute of Technology
R1-11, 4259 Nagatsuta, Midori-ku, Yokohama 226-8503 (Japan)
E-mail: tikeda@res.titech.ac.jp
Dr. H. Yu, Prof. T. Iyoda
The Core Research for Evolutional Science and Technology (CREST)
Japanese Science and Technology Agency (JST)
Kawaguchi Center Building
4-1-8 Honcho, Kawaguchi-shi, Saitama, 337-0017 (Japan)

[**] This work was supported by the Core Research for Evolutional Science and Technology (CREST) from Japanese Science and Technology Agency (JST).

  DOI: 10.1002/adma.200500346